Nat Chem Biol. Author manuscript; available in PMC 2009 October 01.

Published in final edited form as:
Nat Chem Biol. 2009 April ; 5(4): 220–226. doi:10.1038/nchembio.150.

Identification of a chemical probe for NAADP by virtual screening

Edmund Naylor[1,4], **Abdelilah Arredouani**[1,4], **Sridhar R. Vasudevan**[1,4], **Alexander M. Lewis**[1], **Raman Parkesh**[1], **Akiko Mizote**[3], **Daniel Rosen**[1], **Justyn M. Thomas**[1], **Minoru Izumi**[3], **A. Ganesan**[2], **Antony Galione**[1], and **Grant C. Churchill**[1,5]

[1]University of Oxford, Department of Pharmacology, Mansfield Road, Oxford OX1 3QT, United Kingdom.

[2]University of Southampton, Department of Chemistry, Highfield, Southampton, SO17 1BJ, United Kingdom.

[3]Okayama University, Graduate School of Natural Science and Technology, 1-1-1 Tsushimanaka, Okayama 700-8530, Japan

Abstract

Research into the biological role of the Ca^{2+}-releasing second messenger NAADP (nicotinic acid adenine dinucleotide phosphate) has been hampered by a lack of chemical probes. To find new chemical probes for exploring NAADP signaling, we turned to virtual screening, which can evaluate millions of molecules rapidly and inexpensively. We used NAADP as the query ligand to screen the chemical library ZINC for compounds with 3D-shape and electrostatic similarity. We tested the top-ranking hits in a sea urchin egg bioassay and found that one hit, Ned-19, blocks NAADP signaling at nanomolar concentrations. In intact cells, Ned-19 blocked NAADP signaling and fluorescently labeled NAADP receptors. Moreover, we show the utility of Ned-19 as a chemical probe by using it to demonstrate that NAADP is a key causal link between glucose sensing and Ca^{2+} increases in mouse pancreatic beta cells.

NAADP (**1**; nicotinic acid adenine dinucleotide phosphate) is emerging as a crucial Ca^{2+}-releasing second messenger in several mammalian tissues including pancreatic, brain and cardiac1. As NAADP is a relatively new messenger, its mechanism of action and biological roles are either unknown or partially characterized and controversial1,2. In regard to the mechanism of action of NAADP, in sea urchin eggs, where NAADP was first characterized3, low concentrations self-desensitize and higher concentrations activate. This desensitization correlates with a high-affinity binding of NAADP, which is mediated by either more than one binding site or a single site that increases in affinity upon occupancy. This behavior (desensitization and binding) is strikingly analogous to the high-affinity desensitization and agonist trapping of the nicotinic acetylcholine receptor4. In contrast, in mammalian cells, NAADP exhibits a bell-shaped concentration-response relationship5,6. Nevertheless, the same binding model (two site or changing affinity of one site) has been proposed, but with the role of the two sites reversed1,7. Currently, the most controversial topics in NAADP biology are: (1) whether the Ca^{2+} store mobilized by NAADP is a lysosome-related acidic organelle6,8,9 or the endoplasmic reticulum10; (2) whether the NAADP receptor is a novel channel or a known receptor (e.g., the ryanodine receptor)11;

[5] Correspondence: Grant C. Churchill, Email: grant.churchill@pharm.ox.ac.uk.
[4]These authors contributed equally.

Competing financial interests statement
The authors declare competing financial interests: a patent has been filed on the *cis* and *trans* diastereomers of Ned-19.

Europe PMC Funders Author Manuscripts

and (3) whether NAADP plays a redundant or causal role in Ca^{2+}-dependent processes such as glucose sensing in pancreatic beta cells6,9,12.

All the studies described above employed pharmacological manipulation, but either the chemical probes acted indirectly or NAADP itself was used as the sole agonist or antagonist2,3. For example, to shed light on the identity of the Ca^{2+} store, indirectly-acting chemical probes have been extensively used such as bafilomycin (**2**, a H^+-ATPase inhibitor), thapsigargin (**3**, an inhibitor of Ca^{2+} pumps on the endoplasmic reticulum) or glycylphenylalanie 2-naphthylamide (**4**, induces osmotic lysis of lysosomes)2,3. Alternatively, to determine the involvement of NAADP in a biological process, NAADP itself has been used to activate or inactivate its receptor1,5,6,8-10,13,14. A major drawback of using NAADP itself is that it is not membrane permeant, and therefore must be introduced into a cell by a pipette (injection or patch5,6,8-10,12,14) or via liposomes15, which are demanding techniques that limit experiments to one or several cells.

For the NAADP field to progress more rapidly we need chemical probes that directly affect NAADP-mediated Ca^{2+} release that are selective, potent and cell permeant2. To address this problem, we and others have previously employed medicinal chemistry approaches and made minor structural alterations to the NAADP molecule itself16-19 or fragments of NAADP20. This yielded NAADP analogs that revealed structure-activity relationships16-19 20, but the compounds are not membrane permeant or are far less potent than NAADP itself, making them of limited utility for answering the outstanding biological questions described above. A major constraint of a medicinal chemistry approach is the chemical nature of the parent molecule; specifically, for NAADP, the molecule is large (744 Da), flexible (12 rotatable bonds) and highly charged (net charge of 4^-), making it decidedly non-drug-like according to Lipinski's 'Rule of 5' criteria21. In addition to medicinal chemistry, a rational screening approach was carried out with so-called nucleotide mimetics evaluated in a bioassay2,22. Although this revealed that triazine dyes are NAADP agonists2,22 and PPADS (**5**) is an antagonist23 and provided chemical scaffolds unrelated to NAADP2,22, all these compounds violate the drug-like criteria21. Clearly, a better approach is desired to meet not just the needs of the NAADP research community, but also the needs of those working on other biological systems that lack good chemical probes. A possible solution is the use of virtual screening24-28, which is commonly used for drug discovery but underused for finding chemical probes to explore basic biology.

We used ligand-based virtual screening with NAADP as the query molecule to search the ZINC database of compounds for molecules with similar 3-dimensional shape and electrostatics. We purchased the top-ranking commercially-available hits and tested them for their ability to antagonize NAADP-induced Ca^{2+} release in a sea urchin egg homogenates. We found a molecule, Ned-19 (**6**) that was potent, blocked NAADP in intact cells and fluorescently labelled NAADP receptors. To demonstrate the experimental utility of Ned-19, we used it to uncover a key causal link between glucose sensing and Ca^{2+} increases in pancreatic beta cells. We hope Ned-19 will be of great utility in uncovering the physiological roles of NAADP.

Results

Virtual screening strategy

Before starting our screen we had to choose a database and software from an array of choices. We chose ZINC (*Z*inc *I*s *N*ot *C*ommercial) because it is an easy to access large database (2.7 million compounds in 2005) containing only commercially available compounds (no costly syntheses were required)29. ZINC contains biologically relevant representation of molecules that are stripped of counterions and possess realistic

tautomerism, protonation and charge29. We chose OpenEye software (OEChem, version 1.3.4, OpenEye Scientific Software, Inc., Santa Fe, NM, USA, www.eyesopen.com, 2005) due to its cost (free for non-commercial use) and its fast and powerful implementation of three-dimensional shape in generating and comparing conformations30,31.

Our starting point was the NAADP molecule, which is large (744 Da), flexible and of unknown bioactive conformation32. Using a single ligand and with no receptor excludes the use of virtual screening strategies based on common features derived from several active compounds or a virtual molecule inferred from the structure of the receptor24-27. Therefore, the option we chose was to use one of several shape-based strategies, which have been used to hop from one drug-like molecular scaffold to another30,33,34 and proposed for hopping from natural ligands to new chemotypes in a retrospective study35. Our approach is novel in that we were attempting to hop directly from an endogenous messenger (non-drug-like) to a drug-like molecule in a prospective study. This shape-based strategy enabled us to explore a range of possible conformations of NAADP by screening against 40 conformations of NAADP generated with Omega (1.8.1 OpenEye Scientific Software, Fig. 1a). Each compound in the ZINC library (2.7 million) was represented in our screen by up to 100 conformations generated by Omega. An upper limit of 100 was chosen as a previous study reported that a database of 100 and 1,000 conformations provided similar results36.

The three-dimensional shape comparison between NAADP and the molecules in the ZINC library was performed by ROCS (Rapid Overlay of Chemical Structures, version 2.1.1, OpenEye Scientific Software), in which shape is approximated by atom-centered overlapping Gaussians and calculates the maximal intersection of the volume of two molecules30,31,37. ROCS-selected compounds were ranked by their shape Tanimoto score, which is a quantitative measure of three-dimensional overlap where 1 is complete overlap (same shape) and 0.5 would be 50 percent overlap30,31. The top 500 ‘hits’ had Tanimoto scores between 0.66 and 0.73. From a theoretical study, the relative importance of shape and charge varied with the specific biological system31. Therefore, we re-ranked the top 500 compounds for similarity to NAADP based on electrostatics with the program EON (version, 1.1, OpenEye, Scientific Software). Electrostatic rank was based on an electrostatic Tanimoto score, which ranges from one (identical) to negative values resulting from the overlap of positive and negative charges31.

We performed two EON screens. In our initial EON screen we used a single lowest-energy conformer of NAADP for all the electrostatic comparisons. As EON does not shape match, this approach is flawed and can give spurious results. Subsequently, after the first round of review at the journal, we conducted a second EON screen using the NAADP conformer that selected a given ZINC compound (shape matched) for the electrostatic comparisons. In both EON runs, we used NAADP with protonated phosphates, but we did not specify the protonation or charged state of the database molecules. Thus, the net charge was +2 for NAADP and variable for the ZINC molecules. Despite this, in the second EON screen all 14 compounds from the first screen remained in the top 19 in the second screen (Supplementary Table 1). This small effect on the identity and ordering of the hits is surprising because EON is not designed to compare molecules with different net charges and it not clear why this method worked. Following biological characterization of the compounds from the first screen, we purchased and biologically tested the additional compounds from the second screen (Supplementary Table 1 and Fig. 2A). The electrostatic Tanimotos for the 500 ROCS hits in the second EON screen ranged from −0.31 to 0.85. To easily track the pedigrees of the compounds, we labeled hits ranked solely by ROCS ‘Nrd’ for ‘NAADP ROCS discovered’ and those ranked by the second EON screen ‘Ned’ for ‘NAADP EON discovered’, and numbered according to their Tanimoto rank. We selected and purchased the top 10 Nrd hits after the initial EON screen and the top 15 Ned hits (5 new compounds) after

the second EON screen. Full details for these compounds including their structures, properties, Tanimoto ranks and chemical identification numbers are provided in Supplementary Table 1. When a given compound was not available from a supplier, we purchased the next highest-ranking compound. In regard to similarity to NAADP, all the hits from the virtual screen were radically different in regard to their two-dimensional scaffold, but similar in regard to their three-dimensional shape as demonstrated by their shape Tanimotos (Supplementary Table 1). This is clearly illustrated by the hit with the best biological activity (see later), Ned-19 (Fig. 1b), when it is overlapped with NAADP (Fig. 1c) and by its shape Tanimoto of 0.67. Electrostatically, Ned-19 is also similar to NAADP (Fig. 1d) with an electrostatic Tanimoto of 0.65.

Biological testing and hit validation

For biological testing we chose to use the sea urchin egg homogenate for several reasons: our familiarity with it14, its robustness and its well-characterized response to all three Ca^{2+}-releasing second messengers: inositol 1,4,5-trisphosphate (**43**), cyclic ADP-ribose (**44**) and NAADP1,14. We initially screened all the compounds with a plate reader (2-4 replicates) for antagonist activity by quantifying their inhibition of the response to NAADP at its 50 percent effective concentration (EC_{50}). Of the 25 purchased compounds, 23 were tested in the bioassay, as Nrd-7 (**13**) and Nrd-11 (**17**) were sparingly soluble they were not tested. The compounds Nrd-10 (**16**) and Ned-16 (**35**) induced irreversible Ca^{2+} release in the bioassay; hence, we obtained reliable results for the antagonist activity for 21 of the 25 hit compounds (Fig. 2a). Of the 21 testable hit compounds, 4 exhibited significant inhibition (Fig. 2a; one-tailed t-test, $p \leq 0.05$), putting the success of a biologically active hit at about 1:5 compared to 1:5,000 with a random compound in high-throughput screening38.

We focused on Ned-19, as this was the most potent inhibitor of NAADP action (Fig. 2a,b). Ned-19 at 100 μM effectively eliminated NAADP-mediated Ca^{2+} release (5.4±1.0 percent of its control, n=5, p<0.0001), but did not affect either inositol 1,4,5-trisphosphate-mediated Ca^{2+} release (87±5.1 percent of its control, n=4, p=0.08) or cyclic ADP-ribose-mediated Ca^{2+} release (101±6.6 percent of its control, n=4, p=0.93; Fig. 2b). Therefore, Ned-19 was highly selective for NAADP-mediated Ca^{2+} release. The inhibition of NAADP by Ned-19 was concentration-dependent with an IC_{50} (50 percent inhibitory concentration) of 2 μM and a Hill coefficient of −0.6 (Fig. 2c), suggesting more than one class of binding site. This fits with the idea of separate binding sites for activation and inhibition by NAADP7,13,39.

Ned-19 is a noncompetitive antagonist

To determine the type of antagonism exhibited by Ned-19, we obtained concentration-response curves for NAADP in the constant presence of 125 μM Ned-19 (Fig. 2d). Ned-19 reduced the maximum release and shifted the EC_{50} to the right (Fig. 2d) suggesting uncompetitive antagonism. Ned-20 (**38**), a close structural analog in which the fluorine atom is *para* on the benzene ring (Fig. 1b), did not affect the response to NAADP (Fig. 2e). In contrast to NAADP-induced Ca^{2+} release (Fig. 2d), Ned-19 was able to compete fully with [^{32}P]NAADP for binding to the sea urchin egg binding protein with an affinity of 6 μM and a Hill coefficient of −2.3 (Fig. 2f) suggesting competitive binding. These disparate results can be reconciled by the kinetics of Ned-19 binding; only about half the bound Ned-19 dissociates from the NAADP receptor even after 5 days (Fig. 2g), consistent with slow dissociation of NAADP itself7,13,39. Combined, these results suggest that Ned-19 is a functionally irreversible (possibly occluded, but not covalently attached) noncompetitive antagonist of NAADP.

The commercially purchased Ned-19 was mixture of diastereomers as revealed by fluorine nuclear magnetic resonance (Supplementary Fig. 1), reverse-phase high-performance liquid

chromatography (Supplementary Fig. 2) and proton nuclear magnetic resonance (Supplementary Methods). The computer-based shape comparison showed a better 3-dimensional overlap (Fig. 1c) with the *trans* diastereomer when the stereocenter of the cyclic tryptophan is of the L configuration. To test the biological activity of these diastereomers, we used L-tryptophan to synthesize *trans*-Ned-19 (**6a**) and *cis*-Ned-19 (**6b**, Fig. 2h and Supplementary Scheme 1). The *trans* form was more potent than the *cis* form in regard to both inhibition of Ca^{2+} release (IC_{50} of 6 nM versus 800 nM; Fig. 2i) and [^{32}P]NAADP binding (IC_{50} of 0.4 nM versus 15 μM; Fig. 2j). The differences between antagonist potency and binding inhibition is consistent with binding to the NAADP receptor being functionally irreversible (Fig. 2g)7,13,39. This irreversible binding means that pre-incubation shifts the concentration-inhibition curve leftward by about 10-fold in a time-dependent manner7,13,39. For binding, Ned-19 was pre-incubated for 10 min before the addition of [^{32}P]NAADP, whereas for Ca^{2+}-release, Ned-19 was pre-incubated for only 3 min before the addition of NAADP.

Ned-19 blocks NAADP signaling in intact cells

As Ned-19 has a predicted Log P of 3.68 (ChemOffice Ultra), we anticipated that Ned-19 would be cell permeant and thus effective on intact cells. In intact sea urchin eggs incubated in artificial seawater containing 100 μM Ned-19, the injection of NAADP failed to elicit a Ca^{2+} increase compared to the control (Fig. 3a). Hence, the overall virtual screening strategy proved effective in identifying a cell-permeant antagonist of NAADP in the sea urchin egg. The question was then does the antagonist activity extend to a mammalian cell? In mouse pancreatic beta cells, NAADP applied via a patch pipette (50 nM) induced Ca^{2+} spiking as reported previously6,9,12. Pre-incubation with Ned-19 (125 μM) in the bathing solution blocked NAADP-mediated Ca^{2+} spiking (Fig. 3b). Therefore, Ned-19 acts as a cell-permeant antagonist in both sea urchin eggs and in mammalian cells.

Ned-19 fluorescently labels NAADP receptors

As predicted for a derivative of tryptophan (**45**, Fig. 1b), Ned-19 is fluorescent. The excitation and emission spectra (Fig. 4a) indicated that the fluorescence of Ned-19 was compatible with visualization of the NAADP receptor in intact cells via confocal microscopy using an ultraviolet Argon ion laser (excitation 351 and 365 nm). Indeed, Ned-19 labels the NAADP receptor in mouse pancreatic beta cells (Fig. 4b). Dissipation of the lysosomal proton gradient with bafilomycin A1 did not affect Ned-19 localization but eliminated lysotracker red (**46**) labeling (Fig. 4b). Conversely, pre-incubation with cell-permeant NAADP-actetoxymethyl ester (**47**, 60 nM for 30 min), did not eliminate lysotracker red localization but altered the subcellular localization of Ned-19 from punctate and organellar to a diffuse cytoplasmic distribution (Fig. 4b). These results demonstrate that Ned-19 is not acid-trapped in acidic organelles but rather labeling NAADP receptors. The history of fluorescent molecules for probing biology is rich and successful40; therefore, we anticipate that Ned-19 will be of great utility for studying NAADP signaling.

Ned-19 reveals role for NAADP in glucose sensing

Although NAADP releases Ca^{2+} in a pancreatic beta cell line6,12 and isolated human beta cells 41, a causal link between glucose (**48**) sensing and NAADP-induced Ca^{2+} increases remains controversial and unproven. To explore this causal link, we investigated the effects of Ned-19 on glucose-mediated Ca^{2+} signaling. In an acutely isolated islet from mouse pancreas, the addition of glucose (10 mM) resulted in the typical Ca^{2+} signature42 of a decrease in Ca^{2+} followed by large increase with sustained oscillations on an elevated plateau (Fig. 5a). The addition of Ned-19 (100 μM) reduced the amplitude of the oscillations and reduced the elevated plateau to the nonstimulated level (Fig. 5a). In contrast, the close

structural analogue Ned-20 (Fig. 1b) was without effect (Fig. 5b). Ned-19 reduced the amplitude of all aspects of the glucose-induced Ca^{2+} signal: the first peak, the oscillations and the plateau (Fig. 5c) in a concentration-dependent manner with an IC_{50} of 3 μM (Fig. 5d). In these concentration-inhibition experiments, we pre-incubated the islets with Ned-19 for 30 min before the addition of glucose to ensure Ned-19 had reached its intracellular target in islets. To assess the selectivity of Ned-19 for NAADP-induced Ca^{2+} increases relative to other glucose-altered responses, we monitored the effects of Ned-19 on voltage-gated Ca^{2+} channels and mitochondrial metabolism. In islets incubated in the presence of glucose (10 mM to stimulate metabolism) and diazoxide (**49**, 100 μM to open the ATP-sensitive K channels and prevent depolarization), depolarization with KCl (45 mM) resulted in a Ca^{2+} transient that was unaltered by 100 μM Ned-19 (Fig. 5e). Therefore, Ned-19 does not act through inhibition of L-type Ca^{2+} channels. Likewise, a glucose-induced increase in pooled NADH (**50**) and NADPH (**51**) fluorescence still occurred in the presence of 100 μM Ned-19 (Fig. 5f). Therefore, Ned-19 does not act via disruption of mitochondrial metabolism. Taken together, these data show a causal link between NAADP signaling and glucose-induced Ca^{2+} increases and, thereby, demonstrate the utility of Ned-19 as a chemical probe for revealing novel biology.

Discussion

Although genetic techniques are more commonly used than small molecules to probe biological function, small molecules remain sought after for their ability to alter biological function in a rapid, selective, reversible and concentration-dependent manner43. Moreover, small molecules complement genetic approaches and are a means of identifying and validating therapeutic targets43. Our success in using virtual screening to find a small-molecule, cell-permeant antagonist of NAADP is of considerable importance to the fields of virtual screening and NAADP biology.

The received mechanism by which pancreatic beta cells sense glucose and secrete insulin is given as follows: glucose metabolism, increase in ATP, closure of ATP-sensitive K^+ channels44, depolarization-induced activation of Ca^{2+} channels, Ca^{2+} influx-induced exocytosis of insulin-containing vesicles. Nevertheless, this may not be the only mechanism, as *Sur1* knockout mice still secrete insulin in response to glucose45. Sur1 codes for the sulfonylurea receptor, a subunit of the ATP-sensitive K^+ channel and is essential for its function44. Arguments for a mechanism involving the release of Ca^{2+} from intracellular stores exists42, but the actual second messenger(s) remain controversial, with evidence for inositol 1,4,5-trisphosphate46, cyclic ADP-ribose47 and NAADP6,12,41. Amid this controversy, we used Ned-19 to demonstrate a causal link between glucose sensing and NAADP-induced Ca^{2+} increases in pancreatic beta cells, thereby revealing novel biology. Thus, Ned-19 represents a powerful small molecule tool with the potential to enhance greatly research into the roles of NAADP in intracellular Ca^{2+} signaling in health and disease.

Methods

Virtual screening

We performed virtual screening on a computer with an AMD Athlon 64 2.6 GHz processor using SUSE Linux 9.2 operating system with software from OpenEye (OpenEye Scientific Software, Santa Fe, USA) and the chemical database ZINC (http://blaster.docking.org/zinc). We used ChemDraw 3D Ultra (8.0, CambridgeSoft) to draw and energy minimize (with MMFF94) a 3-dimensional conformer of NAADP. We used OMEGA 1.8.1 to generate 40 conformers of NAADP and up to 100 conformers of each ZINC molecule. The input NAADP was entered as a virtual molecule for the screen in that all the oxygen-phosphate

bonds were set to single bonds to approximate the resonance shape of phosphate rather than the conventionally drawn Lewis structure having one double bond and three single bonds. We used ROCS (2.1.1) for 3-dimensional shape comparisons and the 500 molecules with highest shape Tanimoto values were outputted in rank order as hits.

For electrostatic comparisons (EON 1.1), in the first EON screen, a single lowest-energy conformer of NAADP was used for all comparisons to re-rank the top 500 shape-based (ROCS) hits. EON does not perform any shape matching. Therefore, in our first EON screen, we might have obtained anomalous results in which two mismatched shapes were used for electrostatic comparison. To avoid such anomalies, we conducted a second EON screen in which we only used electrostatic Tanimoto scores obtained from the conformer of NAADP that selected the hit conformer during the ROCS screen. The results from the 40 independent runs (one for each NAADP conformer) were pooled and ranked by electrostatic Tanimoto. To prevent a positive charge from being placed on the phosphorous atom, for all phosphates we converted one oxygen-phosphate bond to a double bond. All the phosphates were modeled as fully protonated and neutral because when modeled with charge the electrostatic field was distorted. With neutral phosphates, NAADP had a net positive charge of +2 due to the pyrimidine ring nitrogen and the imino nitrogen, but this did not appear to distort the electrostatics. Note that the time taken for each step (Fig. 1a) is dependent on the particular computer system used and that these times should be taken as upper limits. If the calculations were run in parallel, there would be a dramatic reduction in the time taken.

Biological testing with sea urchin egg homogenates

The top 10 commercially-available ROCS (Nrd) hits and the top 15 commercially-available EON-ranked (Ned) compounds were purchased for testing. We tested the compounds in a bioassay contains sea urchin egg homogenate *(Lytechinus pictus* obtained from Marinus, Long Beach, CA), a Ca^{2+}-reporting fluorescent dye (fluo-3) and ATP14. Compounds were tested for their ability to antagonize the Ca^{2+} release induced by NAADP applied at its EC_{50} concentration (30-50 nM, depending on the homogenate). Initial screens (2-4 replicates) were conducted with a plate reader using 384-well plates and confirmatory tests were conducted with a fluorimeter with 500-μL of homogenate as reported previously14.

Radioligand displacement binding assay

Sea urchin egg homogenate in intracellular-like buffer was added to a range of concentrations of hit compound in dimethylsulfoxide to give a final concentration of 1% (volume volume^{-1}) in 150 μL. After incubation for 10 min at 25°C, [^{32}P]NAADP in intracellular buffer was added to give a concentration of 0.3 nM in a final volume of 250 μL. Samples were incubated for 30 minutes; henceforth [^{32}P]NAADP binding was assessed as described14. To determine the extent of dissociation of NAADP and Ned-19, compounds were pre-incubated with sea urchin egg homogenate for 10 min and then [^{32}P]NAADP was added and the samples were filtered at various time points. The dissociation of the non-radioactive compound is detected by the recovery of binding as binding sites are freed up.

Imaging Ca^{2+} in intact cells

Sea urchin eggs were imaged as described previously14. Eggs were transferred to polylysine-coated glass coverslips, pressure microinjected with Oregon Green 488 BAPTA Dextran. The Ca^{2+}-sensitive dye was imaged by laser-scanning confocal microscopy (Leica) with 488 nm excitation (Ar ion laser) and emission collected with either a 530±15 nm band-pass or 510 nm long-pass filter. NAADP (100 μM in the pipette) was pressure microinjected to one percent egg volume. Pancreatic beta cells were imaged using fura-PE3-acetyoxymethylester.

Imaging NAD(P)H in intact cells

Islets of Langerhans were preincubated for 60 min at 37°C in a control medium containing 3 mM glucose. NAD(P)H (NADH and NADPH) was measured by fluorescence (360 nm excitation and > 470 nm emission). The changes in fluorescence were expressed as a percentage of basal values within the same islet.

Imaging lysosomes and NAADP receptors in intact cells

Acidic organelles were labeled by incubation with 50 nM LysoTracker Red for 20-40 min. Confocal microscopy (as described above) was used to detect LysoTracker Red with excitation at 568 nm (Kr-ion laser) and emission collected above 590 nm with a long-pass filter. Ned-19 was monitored with excitation at 355 nm (Ar-ion laser) and emission collected with a 415±30 nm band-pass filter. The lysosomal pH gradient was disrupted by incubating cells for 15 minutes with bafilomycin A1 (3 μM), a specific inhibitor of the V-type-H^+-pump. NAADP-acetoxymethyl ester was synthesized as reported48. We maintained the same illumination intensity and camera acquisition settings during the capture of images for all the conditions. We used Photoshop (Adobe) to process the all the raw images at once and equally to optimize brightness and contrast and add false color.

Electrophysiology

Patch-clamp measurements were carried out using the standard whole-cell mode of the patch-clamp technique at room temperature, using multiclamp 700B and the software pCalmp 9 (Axon Instruments). Patch pipettes were pulled from borosilicate glass capillaries to give a resistance of 3–5 MΩ when filled with intracellular solution. The holding potential was −70 mV. The intra-pipette solution contained in mM: 125 K-glutamate; 10 KCl; 10 NaCl; 1 $MgCl_2$; 3 MgATP; 0.1 GTP; 1 EGTA, 5 Hepes at pH 7.1.

Statistical tests

Data were analyzed by one-tailed t-tests using Prism 4 (GraftPad Software). Data are presented as mean ± standard error of the mean.

Supplementary Material

Refer to Web version on PubMed Central for supplementary material.

Acknowledgments

Our research was supported by a grant from the Biotechnology and Biological Sciences Research Council [grant number BB/D012694/1]. We thank Dr Paul Hawkins (OpenEye Scientific Software, New Mexico) for advice with virtual screening, Professor Hon-Cheung Lee (University of Hong Kong) for providing ADP-ribosyl cyclase and Clive Garnham (Oxford University) for help with the plate reader.

References

1. Lee HC. Nicotinic acid adenine dinucleotide phosphate (NAADP)-mediated calcium signaling. J. Biol. Chem. 2005; 280:33693–6. [PubMed: 16076847]
2. Galione A, Parrington J, Dowden J. The NAADP receptor: commentary on Billington et al. Br. J. Pharmacol. 2004; 142:1203–7. [PubMed: 15265809]
3. Lee HC, Aarhus R. A derivative of NADP mobilizes calcium stores insensitive to inositol trisphosphate and cyclic ADP-ribose. J. Biol. Chem. 1995; 270:2152–7. [PubMed: 7836444]
4. Giniatullin R, Nistri A, Yakel JL. Desensitization of nicotinic ACh receptors: shaping cholinergic signaling. Trend. Pharm. Sci. 2005; 283:371–378.
5. Cancela JM, Churchill GC, Galione A. Coordination of agonist-induced Ca^{2+}-signalling patterns by NAADP in pancreatic acinar cells. Nature. 1999; 398:74–76. [PubMed: 10078532]

6. Masgrau R, Churchill GC, Morgan AJ, Ashcroft SJ, Galione A. NAADP: a new second messenger for glucose-induced Ca^{2+} responses in clonal pancreatic beta cells. Curr. Biol. 2003; 13:247–51. [PubMed: 12573222]
7. Patel S. NAADP-induced Ca^{2+} release -- a new signalling pathway. Biol. Cell. 2004; 96:19–28. [PubMed: 15093124]
8. Churchill GC, et al. NAADP mobilizes Ca^{2+} from reserve granules, lysosome-related organelles, in sea urchin eggs. Cell. 2002; 111:703–8. [PubMed: 12464181]
9. Yamasaki M, et al. Organelle selection determines agonist-specific Ca^{2+} signals in pancreatic acinar and beta cells. J. Biol. Chem. 2004; 279:7234–40. [PubMed: 14660554]
10. Gerasimenko JV, Sherwood M, Tepikin AV, Petersen OH, Gerasimenko OV. NAADP, cADPR and IP_3 all release Ca^{2+} from the endoplasmic reticulum and an acidic store in the secretory granule area. J. Cell Sci. 2006; 119:226–38. [PubMed: 16410548]
11. Galione A, Petersen OH. The NAADP receptor: new receptors or new regulation? Mol. Interv. 2005; 5:73–9. [PubMed: 15821155]
12. Mitchell KJ, Lai FA, Rutter GA. Ryanodine receptor type I and nicotinic acid adenine dinucleotide phosphate receptors mediate Ca^{2+} release from insulin-containing vesicles in living pancreatic beta-cells (MIN6). J. Biol. Chem. 2003; 278:11057–64. [PubMed: 12538591]
13. Genazzani AA, Empson RM, Galione A. Unique inactivation properties of NAADP-sensitive Ca^{2+} release. J. Biol. Chem. 1996; 271:11599–602. [PubMed: 8662773]
14. Morgan, AJ., et al. Methods in cyclic ADP-ribose and NAADP research. In: Putney, JWJ., editor. Methods in Calcium Signalling. CRC Press; Boca Raton: 2006. p. 265-333.
15. Brailoiu E, et al. Nicotinic acid adenine dinucleotide phosphate potentiates neurite outgrowth. J. Biol. Chem. 2005; 280:5646–5650. [PubMed: 15528210]
16. Billington RA, et al. Production and characterization of reduced NAADP (nicotinic acid-adenine dinucleotide phosphate). Biochem. J. 2004; 378:275–80. [PubMed: 14606955]
17. Billington RA, Tron GC, Reichenbach S, Sorba G, Genazzani AA. Role of the nicotinic acid group in NAADP receptor selectivity. Cell Calcium. 2005; 37:81–6. [PubMed: 15541466]
18. Lee HC, Aarhus R. Structural determinants of nicotinic acid adenine dinucleotide phosphate important for its calcium-mobilizing activity. J. Biol. Chem. 1997; 272:20378–83. [PubMed: 9252343]
19. Lee HC, Aarhus R. Fluorescent analogs of NAADP with calcium mobilizing activity. Biochim. Biophys. Acta. 1998; 1425:263–71. [PubMed: 9813359]
20. Dowden J, et al. Cell-permeant small-molecule modulators of NAADP-mediated Ca^{2+} release. Chem. Biol. 2006; 13:659–65. [PubMed: 16793523]
21. Lipinski CA, Lombardo F, Dominy BW, Feeney PJ. Experimental and computational approaches to estimate solubility and permeability in drug discovery and development settings. Adv. Drug Deliver. Rev. 1997; 23:3–25.
22. Billington RA, Bak J, Martinez-Coscolla A, Debidda M, Genazzani AA. Triazine dyes are agonists of the NAADP receptor. Br. J. Pharmacol. 2004; 142:1241–6. [PubMed: 15265807]
23. Billington RA, Genazzani AA. PPADS is a reversible competitive antagonist of the NAADP receptor. Cell Calcium. 2007; 41:505–11. [PubMed: 17084890]
24. Jorgensen WL. The many roles of computation in drug discovery. Science. 2004; 303:1813–1818. [PubMed: 15031495]
25. Oprea TI, Matter H. Integrating virtual screening in lead discovery. Curr. Opin. Chem. Biol. 2004; 8:349–58. [PubMed: 15288243]
26. Shoichet BK. Virtual screening of chemical libraries. Nature. 2004; 432:862–865. [PubMed: 15602552]
27. Drews J. Drug Discovery: A Historical Perspective. Science. 2000; 287:1960–1964. [PubMed: 10720314]
28. Tuma R. Discovering therapeutics through virtual screening. Drug Discov. Dev. 2005
29. Irwin JJ, Shoichet BK. ZINC--a free database of commercially available compounds for virtual screening. J. Chem. Inf. Model. 2005; 45:177–82. [PubMed: 15667143]

30. Rush TS 3rd, Grant JA, Mosyak L, Nicholls A. A shape-based 3-D scaffold hopping method and its application to a bacterial protein-protein interaction. J. Med. Chem. 2005; 48:1489–95. [PubMed: 15743191]
31. Nicholls A, MacCuish NE, MacCuish JD. Variable selection and model validation of 2D and 3D molecular descriptors. J. Comp. Aid. Mol. Design. 2004; 18:451–474.
32. Galione A, Ruas M. NAADP receptors. Cell Calcium. 2005; 38:273–80. [PubMed: 16111747]
33. Boström J, Berggren K, Elebring T, Greasleya PJ, Wilstermanna M. Scaffold hopping, synthesis and structure–activity relationships of 5,6-diaryl-pyrazine-2-amide derivatives: a novel series of CB1 receptor antagonists. Bioorg Med Chem. 2007; 15:4077–4084. [PubMed: 17433696]
34. Hawkins PCD, Skillman AG, Nicholls A. Comparison of shape-matching and docking as virtual screening tools. J. Med. Chem. 2007; 50:74–82. [PubMed: 17201411]
35. Jenkins JL, Glick M, Davies JW. A 3D similarity method for scaffold hopping from known drugs or natural ligands to new chemotypes. J. Med. Chem. 2004; 47:6144–59. [PubMed: 15566286]
36. Boström J, Greenwood JR, Gottfries J. Assessing the performance of OMEGA with respect to retrieving bioactive conformations. J. Mol. Graph. Model. 2003; 21:449–62. [PubMed: 12543140]
37. Grant JA, Gallardo MA, Pickup BT. A fast method of molecular shape comaprison: a simple application of a Gaussian description of molecular shape. J. Comput. Chem. 1996; 17:1653–1666.
38. Doman TN, et al. Molecular docking and high-throughput screening for novel inhibitors of protein tyrosine phosphatase-1B. J. Med. Chem. 2002; 45:2213–21. [PubMed: 12014959]
39. Aarhus R, et al. Activation and inactivation of Ca^{2+} release by $NAADP^{+}$ J. Biol. Chem. 1996; 271:8513–6. [PubMed: 8621471]
40. Giepmans BN, Adams SR, Ellisman MH, Tsien RY. The fluorescent toolbox for assessing protein location and function. Science. 2006; 312:217–24. [PubMed: 16614209]
41. Johnson JD, Misler S. Nicotinic acid-adenine dinucleotide phosphate-sensitive calcium stores initiate insulin signalling in human beta cells. Proc. Natl. Acad. Sci. USA. 2003; 99:14566–14571. [PubMed: 12381785]
42. Arredouani A, Henquin JC, Gilon P. Contribution of the endoplasmic reticulum to the glucose-induced Ca^{2+} response in mouse pancreatic islets. Am. J. Physiol. Endocrinol. Metab. 2002; 282:E982–91. [PubMed: 11934662]
43. Tan DS. Diversity-orientated synthesis: exploring the intersections between biology and chemistry. Nat. Chem. Biol. 2005; 1:74–84. [PubMed: 16408003]
44. Ashcroft FM, Harrison DE, Ashcroft SJ. Glucose induces closure of single potassium channels in isolated rat pancreatic beta-cells. Nature. 1984; 312:446–8. [PubMed: 6095103]
45. Seghers V, Nakazaki M, DeMayo F, Aguilar-Bryan L, Bryan J. Sur1 knockout mice. A model for K_{ATP} channel-independent regulation of insulin secretion. J. Biol. Chem. 2000; 275:9270–7. [PubMed: 10734066]
46. Islam MS, Larsson O, Berggren PO. Cyclic ADP-ribose in beta cells. Science. 1993; 262:584–6. [PubMed: 8211188]
47. Takasawa S, Nata K, Yonekura H, Okamoto H. Cyclic ADP-ribose in insulin secretion from pancreatic beta cells. Science. 1993; 259:370–3. [PubMed: 8420005]
48. Parkesh R, et al. Cell-permeant NAADP: A novel chemical tool enabling the study of Ca^{2+} signalling in intact cells. Cell Calcium. 2007; 43:531–538. [PubMed: 17935780]

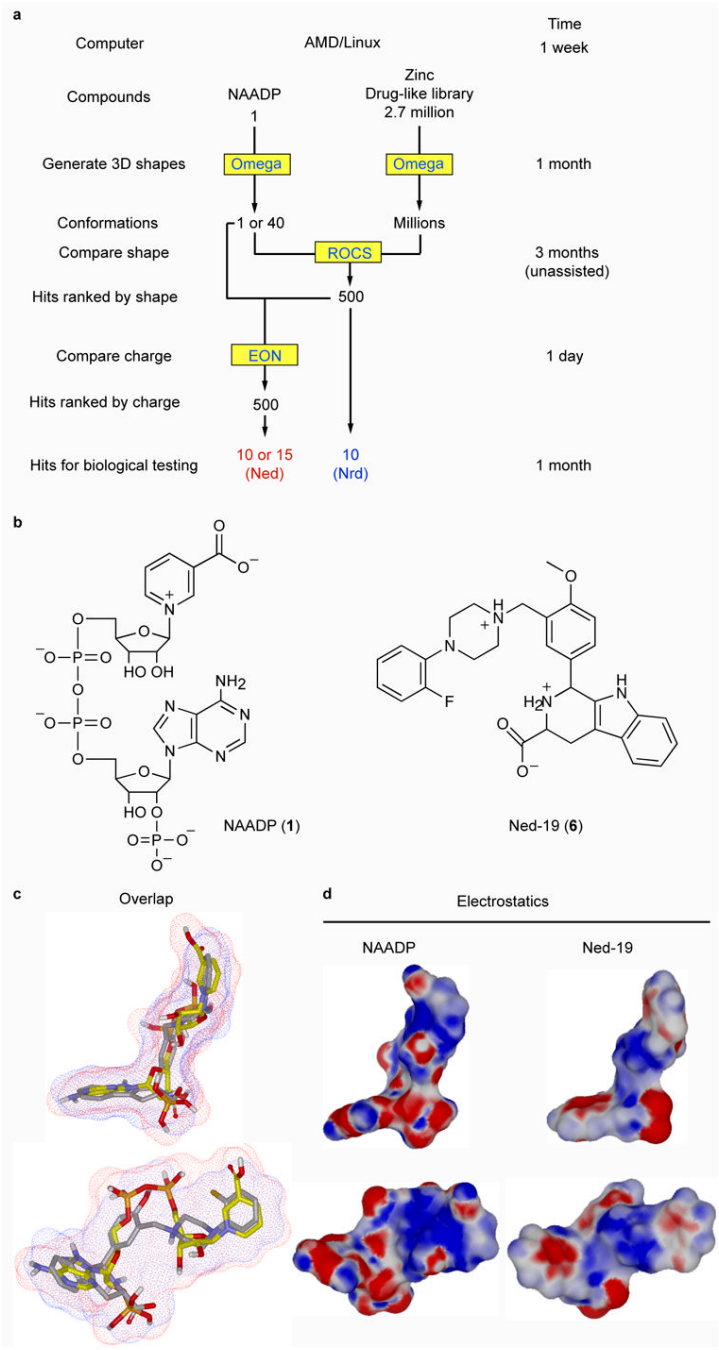

Figure 1.

Strategy and results of a ligand-based virtual screen for drug-like molecules with NAADP-like activity. (**a**) Flow chart outlining the process of ligand-based virtual screening showing the steps (left column), software (yellow boxes), number of compounds and time taken (upper limits on a single computer). (**b**) Two-dimensional chemical structures of NAADP and Ned-19. (**c**) Overlay of NAADP (yellow carbons and red surface) and Ned-19 (grey carbons blue surface). (**d**) Three-dimensional chemical structures of NAADP and Ned-19 with electrostatic surfaces coded by color (red for negative and blue for positive).

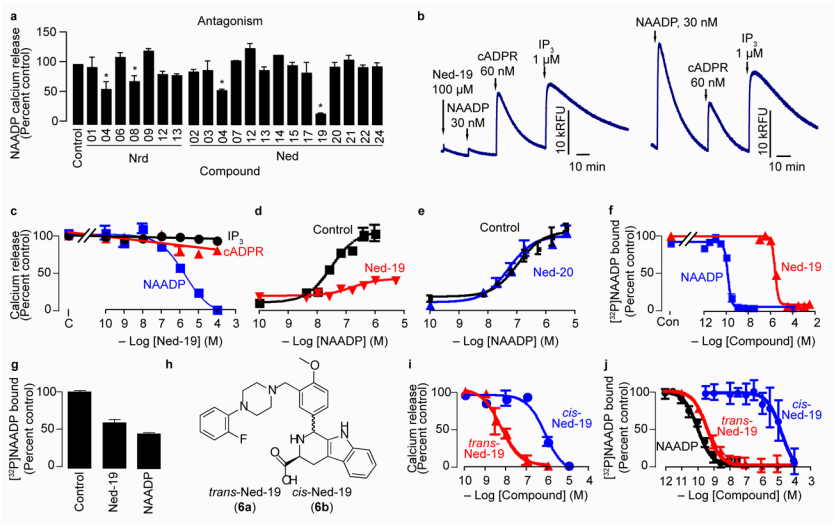

Figure 2.

Certain virtual screening hits have biological activity. (**a**) Relative antagonist activity of the hit compounds against NAADP-mediated Ca^{2+} release. Bars with an asterisk indicate inhibition significantly less than the control based on a one-tailed t-test with $p \leq 0.05$. Hit compounds were present at 6-125 μM depending on their aqueous solubility (see Supplementary Methods) and NAADP was added at its EC_{50} (35 nM). (**b**) The virtual screening hit Ned-19 selectively inhibits NAADP-mediated Ca^{2+} release in a Ca^{2+}-mobilizing bioassay (sea urchin egg homogenate; left panel). All three Ca^{2+}-releasing second messengers release sequestered Ca^{2+} in the control when added at their half-maximal concentration (right trace). Traces show the fluorescence (Relative Fluorescence Units, RFU) from the Ca^{2+}-reporting dye fluo-3. (**c**) Concentration-inhibition curves for Ned-19 on Ca^{2+} release mediated by the EC_{50} concentrations of inositol 1,4,5-trisphosphate (IP_3; 1 μM), cyclic ADP-ribose (cADPR; 300 nM) and NAADP (35 nM). (**d,e**) Concentration-inhibition curves for the compounds Ned-19 (100 μM) (**d**) and Ned-20 (100 μM) (**e**) on NAADP-mediated Ca^{2+} release. (**f**) The compound Ned-19 competes with [^{32}P]NAADP binding. "Con" is the amount of binding in the control. (**g**) Dissociation of Ned-19 (10 μM) and NAADP (10 nM) determined by the recovery of [^{32}P]NAADP binding after 5 days of incubation. A value of 100 percent corresponds to about 1,500 counts per min. (**h**) Chemical structures of the '*trans*' and '*cis*' diastereomers of Ned-19. (**i**) Concentration-inhibition curves for Ned-19 inhibition of NAADP-medicated Ca^{2+} release. (**j**) Concentration-inhibition curves for Ned-19 on [^{32}P]NAADP binding.

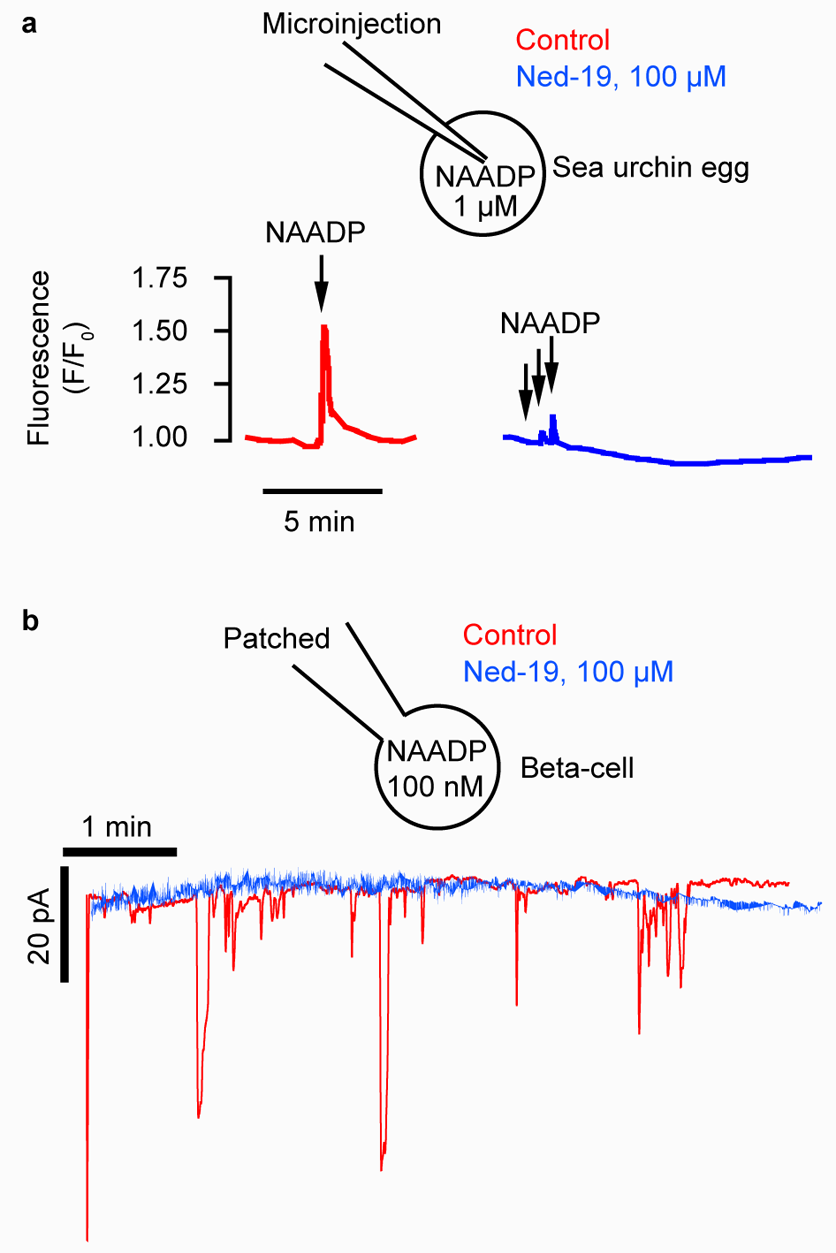

Figure 3.

The virtual screening hit Ned-19 antagonizes Ca^{2+} signaling in intact cells. (**a**) Ned-19 (100 μM in the bath) inhibits NAADP-induced Ca^{2+} release in an intact sea urchin egg. Ca^{2+} was monitored with the Ca^{2+}-reporting dye Oregon Green 488-BAPTA Dextran (10 μM, microinjected). NAADP was pressure microinjected (100 μM in the pipette) so that each injection delivered approximately 1 μM. (**b**) Ned-19 inhibits NAADP-induced Ca^{2+} increases in mouse pancreatic beta cells. Ca^{2+}-dependent current traces are from beta cells that were voltage-clamped with a patch pipette containing 100 nM NAADP in the presence or absence of 100 μM Ned-19 in the bath.

Europe PMC Funders Author Manuscripts

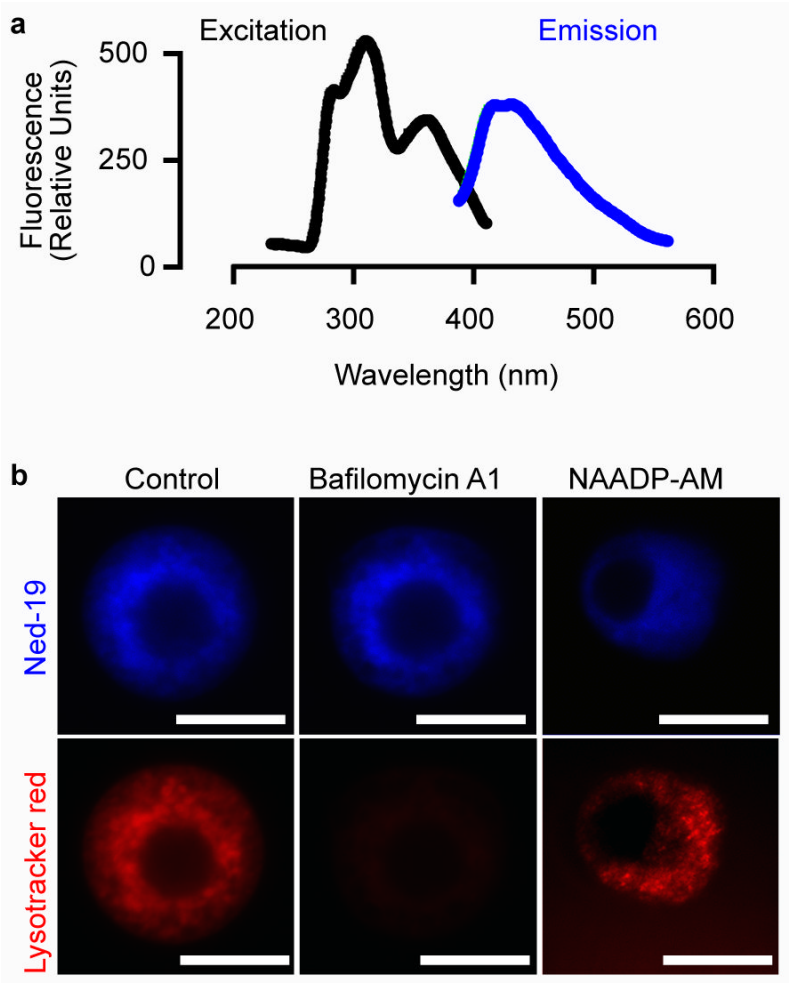

Figure 4.

The virtual screening hit Ned-19 is fluorescent and labels receptors in intact cells. (**a**) Excitation (368 nm) and emission (425 nm) spectra of Ned-19. Ned-19 was in dimethylsulfoxide at 4 mM. (**b**) Ned-19 but not Lysotracker Red labeling of pancreatic beta cells is resistant to the V-type proton pump inhibitor bafilomycin A1. Lyostracker red but not Ned-19 labeling is resistant to pre-treatment with NAADP-acetyoxymethyl ester (NAADP-AM). Scale bars, 5 μm.

Europe PMC Funders Author Manuscripts

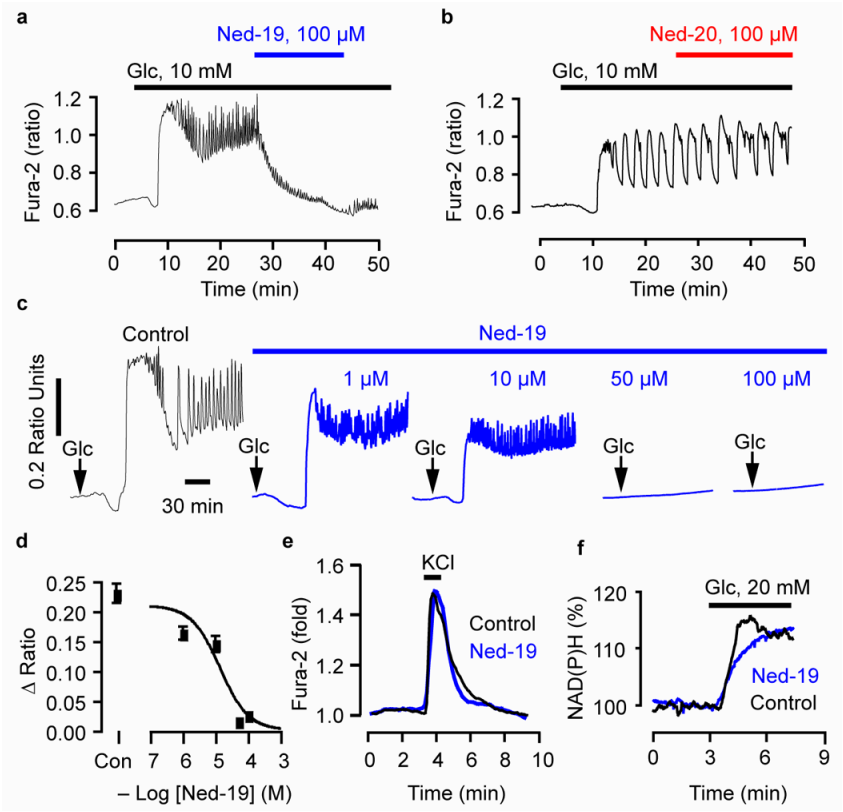

Figure 5.

The virtual screening hit Ned-19 reveals that glucose-induced Ca^{2+} increases require NAADP signaling. (**a**) Ned-19 inhibits glucose-induced Ca^{2+} oscillations. (**b**) Ned-20 does not affect glucose-induced Ca^{2+} increases. (**c,d**) Ned-19 reduces glucose-induced Ca^{2+} increases in a concentration-dependent manner. Islets were pre-incubated with the indicated concentration of Ned-19 for 30 min before the addition of 15 mM glucose. “Con” is the control. (**e**) Ned-19 does not affect the activation of voltage-gated Ca^{2+} channels. Cells were incubated in glucose (10 mM) and diazoxide (100 μM) and then depolarized with KCl (45 mM) in the presence and absence of Ned-19 (100 μM). (**f**) Ned-19 does not interfere with mitochondrial production of NAD(P)H. All cells were maintained in 3 mM glucose unless otherwise indicated.

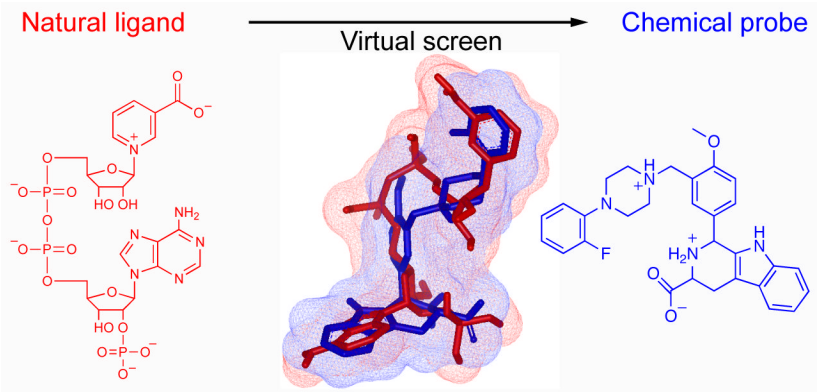

Figure 6.

Europe PMC Funders Author Manuscripts